JOURNAL OF MATERIALS SCIENCE 33 (1998) 1465–1473

Characterization of Nicalon fibres with varying diameters

Part I *Strength and fracture studies*

S. T. TAYLOR*, Y. T. ZHU, W. R. BLUMENTHAL, M. G. STOUT, D. P. BUTT, T. C. LOWE
Mail Stop G755, Materials Science and Technology Division, Los Alamos National Laboratory, Los Alamos, NM 87545 USA
E-mail: yahu@lanl.gov

Experimental studies have been conducted to examine the strength and fracture behaviour of monofilament Nicalon SiC fibres with diameters ranging from 8 to 22 μm. The effects of varying fibre diameter, flaw location and flaw population on the mechanical response of individual fibres were investigated by recourse to extensive fractographic analysis performed on fibres fractured under tensile loading. Results indicate that variations in fibre diameter influence the apparent fibre fracture toughness (K_{1c}), with higher K_{1c} values observed for decreasing fibre diameters. Observations also suggest that the location of the critical flaw may play a role in the fracture of Nicalon fibres. Tensile strength values are shown to increase as the normalized distance of the critical flaw from the fibre centre increases, while critical flaw population appears to be strongly dependent on location. The ratio of K_{1c} to geometry factor (Y) is observed to remain constant with varying flaw location. In addition to surface flaws, three distinct internal flaw populations are seen to cause fracture in Nicalon fibres. Based on these experimental findings, a statistical characterization of the strength of Nicalon fibres with varying diameters is presented in Part II of this paper.

1. Introduction

The challenge to create structural materials with improved high temperature mechanical properties has spawned extensive research into ceramic fibre-reinforced composites in recent years. Owing to their high strength, high Young's modulus, excellent resistance to oxidation, and broad commercial availability, Nicalon™ SiC fibres represent an attractive reinforcement material for elevated-temperature structural components [1–7]. To date, these fibres have found extensive use as reinforcements in metal–, glass– and ceramic–matrix composites for potential use in high temperature applications [8–15].

The mechanical properties of the reinforcing fibres can significantly influence the fracture behaviour of the composite. Fibre strength and strength variability govern not only composite toughening mechanisms such as load transfer, stress accommodation and fibre pull-out [10], but also influence the ultimate strength and other mechanical properties of the composite [8]. Thus, there is a critical need to examine and understand the mechanical behaviour of individual fibres in order to design and develop improved high-performance composites. Determining the strength and fracture behaviour of Nicalon fibres at ambient conditions is particularly important, as these findings provide a fundamental understanding of the various parameters and processes that contribute to fibre fracture. Such findings are ultimately useful in evaluating changes in the mechanical behaviour of the fibres which tend to occur with thermal exposure, composite processing and fibre handling.

The strength and fracture behaviour of Nicalon fibres at ambient conditions have been studied extensively in recent years [1, 9, 16–20]. A comprehensive analysis of strength, structure and fracture relationships was provided by Sawyer *et al.* [20], who demonstrated that fibre tensile strength was controlled by critical flaws. Prominent mirror, mist and hackle regions, typical of brittle fracture, were clearly identified on fracture surfaces. At least three distinct flaw populations were identified in the fractured fibres, and individual populations were shown to correlate with specific strength ranges. Moreover, experimental findings confirmed a volume-based strength dependence for fibres tested at varying gauge lengths and at fixed gauge lengths with varying fibre diameters. Tensile strength was observed to increase with decreasing fibre diameter and with decreasing sample gauge length. However, despite recognizing a

**Present address*: Department of Materials Science and Mineral Engineering, University of California, Berkeley, CA 94720, USA.

diameter-dependence of strength, the authors did not examine the effects of varying fibre diameter on other mechanical properties and fracture characteristics of the fibres. The effects of critical flaw location on fibre fracture behaviour were similarly ignored.

The gauge length-dependence of strength is well documented for Nicalon fibres, but only a few studies have noted a similar dependence of strength on fibre diameter for fibres obtained from the same process batch [9, 16, 21]. Ceramic fibres derived from polymeric precursors and processed via spinning techniques typically show a broad range of fibre diameters within a given tow of fibres. Previous studies have documented this behaviour for Nicalon [1, 9, 13, 14, 16, 20–22] as well as other ceramic fibres [23]. Given the broad distribution of fibre diameters which may exist in a fibre tow, the possible effects of varying fibre diameter on fracture behaviour demand serious consideration. To date, however, no such studies have been performed with these goals in mind.

Part I of this investigation has been conducted in an attempt to identify the effects of varying fibre diameter on the fracture of Nicalon fibres at ambient conditions. Extensive fractographic analysis is used to correlate specific fracture parameters, such as the fracture mirror size and the critical flaw size, with tensile strength data for individual fibres obtained from the same tow, but varying significantly in diameter. These data are used to characterize the apparent fibre fracture toughness and the effective specimen geometry factor with fibre diameter. The effects of critical flaw location and individual flaw populations on strength and fracture properties of the fibres are also addressed. Part II of this paper presents a theoretical treatment of the statistical characterization of strength in fibres with varying diameters. A modified Weibull distribution is proposed to characterize strength for fibres varying significantly in diameter.

2. Experimental procedure

Individual ceramic-grade Nicalon™ SiC fibres with polyvinylalcohol (PVA) sizing (Dow Corning) were separated from a tow of fibres and glued at the ends onto 600-grit sandpaper mounts. Caution was used in handling the fibres so as not to induce any extraneous flaws along the fibre gauge length during the separation procedure. Fibres were selected from varying regions of the tow to maximize sampling volume. Mounted fibres were mechanically secured into an alignment jig which was then attached to the grips of a micro-tensile test machine (MicroPull Science, Thousand Oaks, CA). The MicroPull configuration consists of a load cell, a hydraulically-driven stepper motor, and a linear voltage displacement transducer (LVDT) to measure displacement. Fibres were loaded in tension at a constant displacement rate of $0.3\,\mathrm{mm\,min^{-1}}$ until fracture occurred. Load–displacement curves were measured on a personal computer using software provided with the testing equipment. Peak load and measured cross-sectional area values were used to calculate fibre strength.

Fibres were strength-tested at three different gauge lengths (10, 25 and 50 mm) in mineral oil, with data sets for each gauge length consisting of approximately 50 individual fibre tests. Tests conducted in mineral oil permit consistent recovery of the fractured fibre ends for fractographic analysis on a scanning electron microscope (SEM). Fibres broken in oil were recovered as two distinct fractured ends, and were subsequently rinsed with ethanol, dried in air, and mounted onto aluminium stubs in matched pairs with the fracture surfaces facing up. Fibres breaking outside of the gauge length, or at the extreme ends of the fibre, were discarded. A Jeol 6300FVX SEM was then used to measure fibre diameter and to examine the fracture surface characteristics of each fibre. Since many of the fibre cross-sections were not perfectly circular, four different measurements were made on the fracture surface of each fibre, and their average was taken as the fibre diameter. When possible, the fracture mirror size, critical flaw size and normalized flaw location (defined as the radial distance of the critical flaw from the fibre centre, divided by the fibre radius) were determined for each fibre.

3. Results

Fig. 1 shows the distribution of fibre diameters for all samples tested in mineral oil. Individual fibre diameters vary significantly within the tow, ranging from approximately 8 to 22 μm. From this distribution, the average fibre diameter is calculated as 15.5 μm.

Complex stress states exist near the secured ends of a loaded fibre due to the rigid constraints, or "clamping", of the glue. Stress concentrations arising from this clamping can lead to fracture near or at the fibre ends at anomalously low applied loads. The implication of this end-effect is that some fibres in the total sample population will fail as a result of shortcomings in the test procedure and not because of critical flaw populations. Strength data may not accurately reflect the actual strength of the fibres if the clamping effect is not properly treated [24]. Testing in mineral oil permits recovery of the fractured fibres, so that the location of failure can be determined and samples failing at the fibre ends, or outside of the gauge length, can be discarded. This serves to greatly reduce, though not completely eliminate, the influence of the end-effect on the experimental data. Fig. 2 shows the percentage of

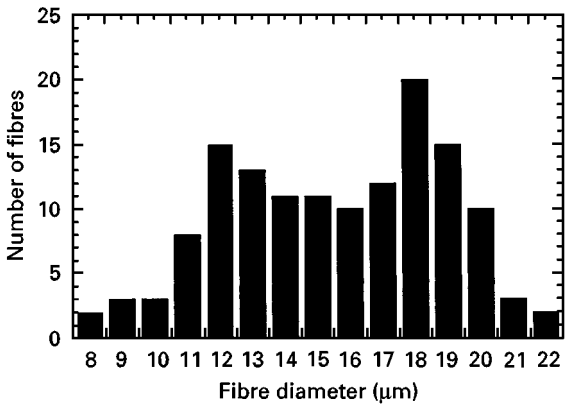

Figure 1 Distribution of fibre diameters for total sample population shows significant variation in diameter.

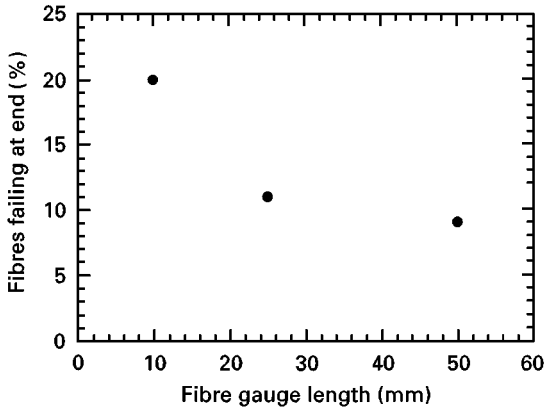

Figure 2 Percentage of fibres failing due to observed end effects plotted as a function of fibre gauge length.

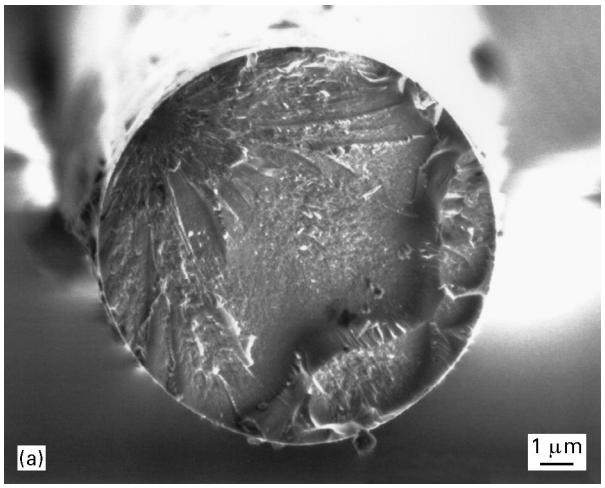

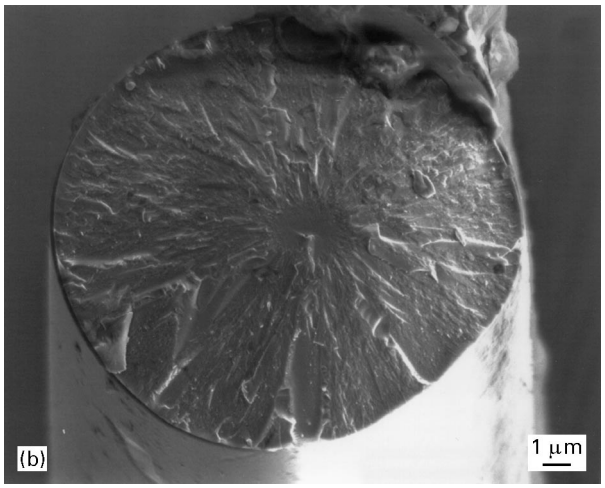

Figure 3 Characteristic fracture surfaces for fibres failing due to (a) surface and (b) interior flaws.

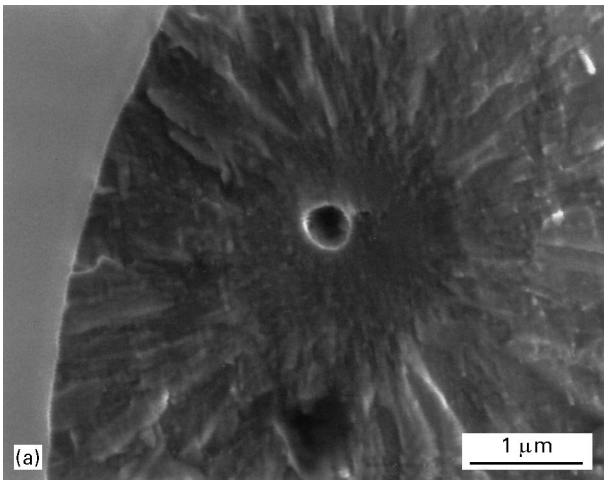

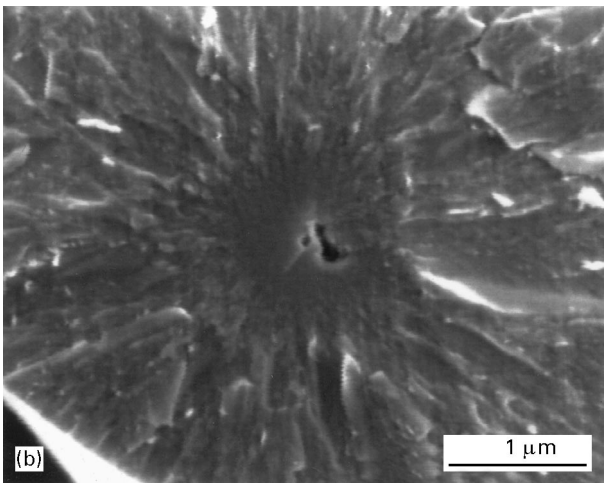

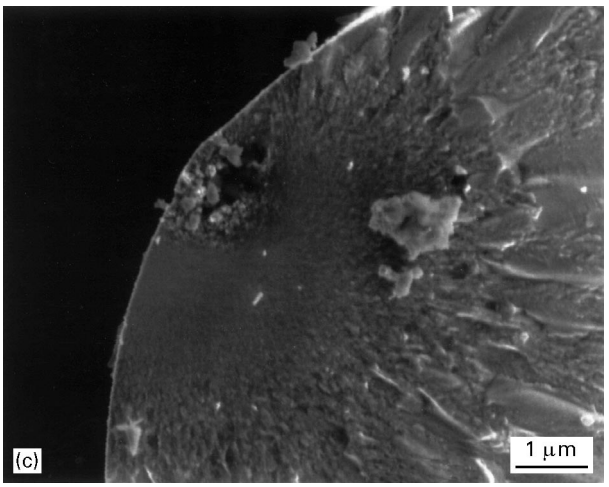

Figure 4 Representative micrographs of the (a) individual pore, (b) pore cluster and (c) granular defect acting as critical flaws.

tested samples failing at the fibre ends as a function of fibre gauge length. As mentioned previously, approximately 50 fibres were tested at each gauge length. The clamping effect is magnified at shorter gauge lengths as a greater fraction of the total fibre length is subjected to the end stresses [25].

Fig. 3a and b show typical fracture surface features for fibres failing because of surface and interior flaws, respectively. The characteristic mirror, mist and hackle features are clearly evident in these micrographs. Fractographic analysis of the fractured fibres reveals that interior flaws can be grouped according to three distinct flaw populations: individual pores, pore clusters, and granular defects. Representative SEM micrographs of each flaw type are presented in Fig. 4. Pore clusters (Fig. 4b) represent collections of small, individual pores which, as demonstrated later, tend to behave as a single collective flaw. Granular

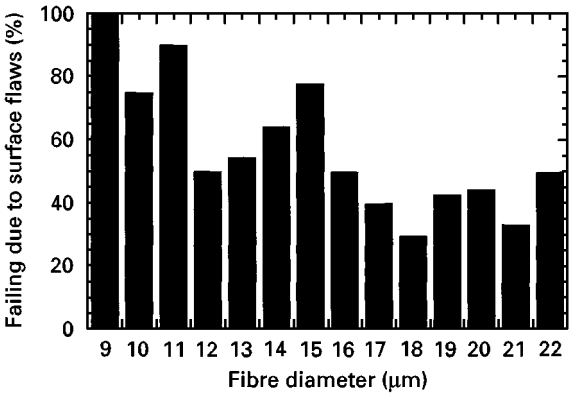

Figure 5 Percentage of fibres failing due to surface flaws as a function of fibre diameter.

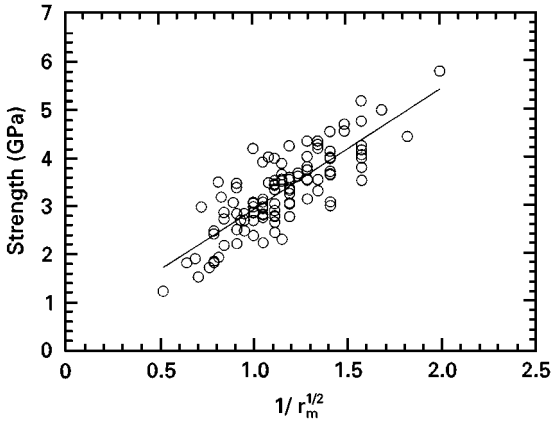

Figure 6 Strength versus the reciprocal square root of mirror radius.

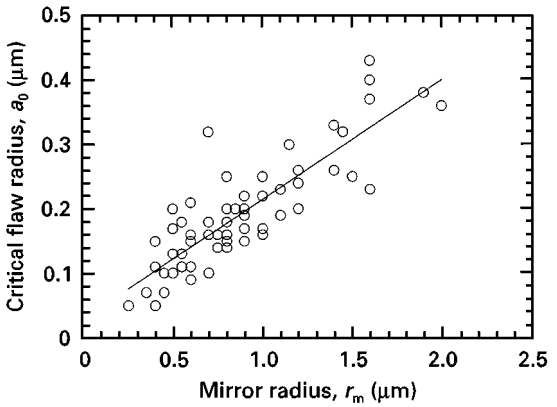

Figure 7 Critical flaw radius plotted as a function of mirror radius showing a definite linear relationship. $a_0/r_m = 0.19$.

defects (Fig. 4c) can be classified as aggregates of small granular particles, which have been shown to be richer in carbon than the bulk fibre [20].

Fig. 5 shows the percentage of fibres failing due to surface flaws as a function of fibre diameter. As the data suggests, smaller fibres are more likely to fail from surface flaws due to their larger surface-area-to-volume ratios. Surface-area-to-volume ratio scales as a factor of $1/r$ for cylindrical fibres, where r is the fibre radius. The relationship depicted in Fig. 5 is consistent with that predicted by statistical theory for fibres failing because of surface flaws.

A dependence of strength on fracture mirror size is common in many glass and polycrystalline ceramic materials [26–32], and is characterized by the empirical relation

$$\sigma_f \sqrt{r_m} = A_m \quad (1)$$

where σ_f is the tensile stress at fracture, r_m is the mirror radius as measured on the fracture surface, and A_m is the mirror constant which is related to the fracture toughness of the material. Strength is plotted as a function of the reciprocal square root of the mirror radius ($1/r_m^{1/2}$) in Fig. 6 for all fibres tested in mineral oil. The slope of this plot yields a mirror constant value of 2.51 MPa $m^{1/2}$, which is consistent with A_m values of 2.51 MPa $m^{1/2}$ [11], 2.0 MPa $m^{1/2}$ [20], and 1.81 MPa $m^{1/2}$ [14] reported previously for Nicalon fibres.

Although not all fibres exhibited such well-defined fracture features as shown in Fig. 3, most fibres displayed a clear, measurable mirror zone, and many fibres permitted accurate assessment of the critical flaw size. However, determination of the flaw size is ultimately a more difficult procedure than the measurement of fracture mirror zones, as flaw sizes can often exceed the resolution of the measuring device. Others [33, 34] have predicted and demonstrated that a flaw-to-mirror size relationship exists for brittle materials, which is material dependent. As Fig. 7 illustrates, a definite relationship exists between the flaw size and the mirror radius for SiC fibres examined in this study. The flaw-to-mirror size ratio obtained here ($a_0/r_m = 0.19$) is very similar to that reported previously (0.22) for Nicalon fibres [10]. Empirical evidence relating mirror size and flaw size is critical to the study of fracture processes in fibrous materials, as mirror zone size measurements can ultimately lend insight to the critical flaw dimensions of brittle fibres when the flaws cannot be directly identified.

Having established a relationship between the critical flaw size and the fracture mirror size, a correlation between the fracture mirror constant (A_m) and the apparent fracture toughness (K_{1c}) can be derived from [35]

$$\sigma_f a_c^{1/2} Y = K_{1c} \quad (2)$$

where a_c is the critical flaw radius, Y is a geometry factor which is dependent on the flaw size and shape and the specimen geometry. The apparent fracture toughness K_{1c} instead of plane strain fracture toughness K_{Ic} is used in Equation 2 because the plane strain condition may not be satisfied at the crack tip because of the small dimension of fibre diameter [35]. The geometry factor Y is presumed to be a function of both the flaw-to-fibre-size ratio (a_c/r) and the flaw location (λ) within the fibre, where λ is defined as the distance from the critical flaw centre to the fibre centre, divided by the fibre radius. Using this convention, the fibre centre is defined as $\lambda = 0$, while the fibre surface is represented by $\lambda = 1$. Substituting $a_c = 0.19 r_m$ (see Fig. 7) into Equation 2 yields

$$\sigma_f r_m^{1/2} Y' = K_{1c} \quad (3)$$

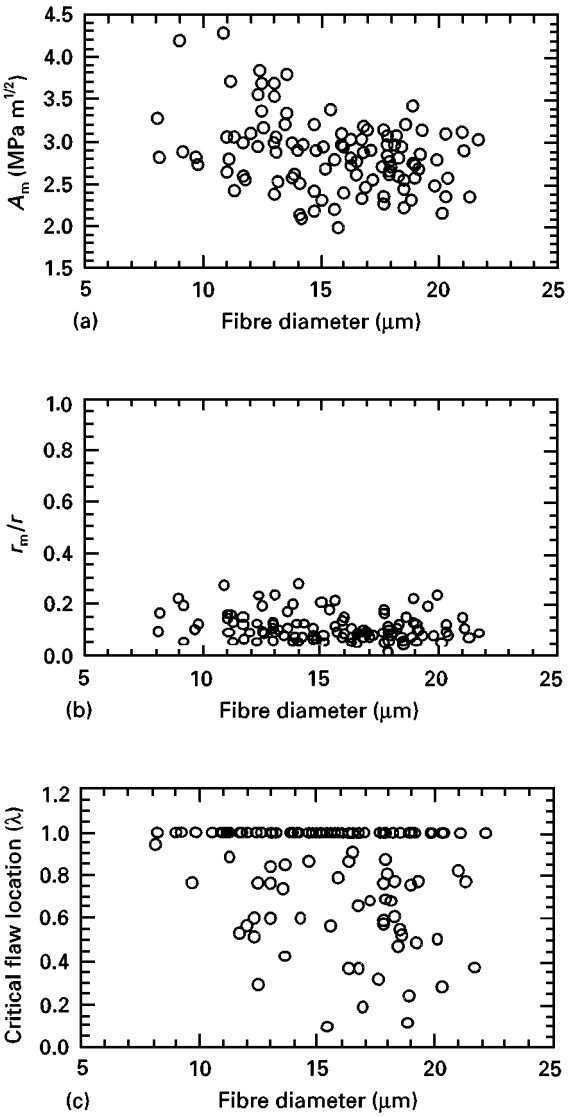

Figure 8 (a) Mirror constant, (b) mirror-to-fibre size ratio and (c) critical flaw location plotted against fibre diameter.

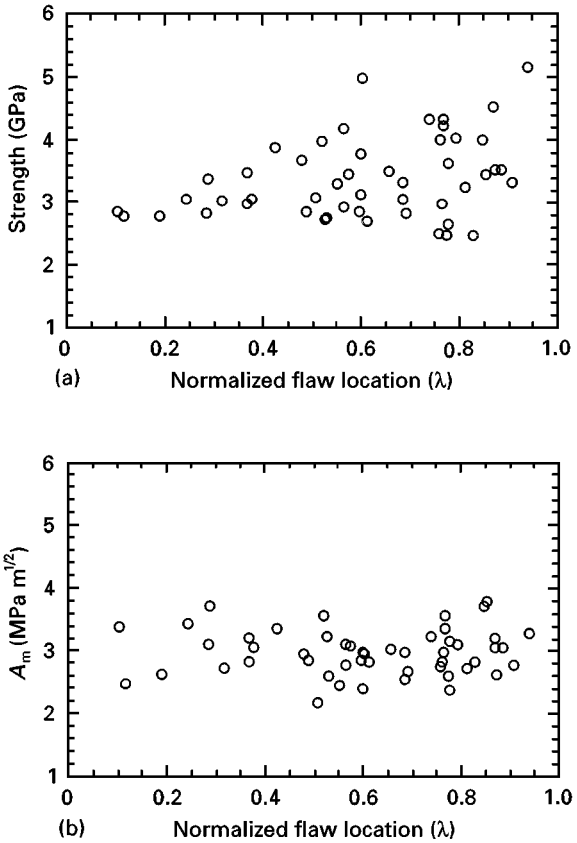

Figure 9 (a) Strength and (b) mirror constant as a function of the normalized critical flaw location.

where $Y' = 0.436\ Y$, and Y' is now a function of r_m/r and λ. Utilizing Equation 1, we see that

$$A_m Y' = K_{1c} \tag{4}$$

and the relationship between mirror constant and fracture toughness is established. Note that the dependence of Y on flaw size a_0 is negligibly small if $a_c/r \ll 1$, so that a dependence of Y' on r_m/r can also be ignored if $r_m/r \ll 1$. Because no direct measurements of Y' or K_{1c} have been made for glass or ceramic fibres of such small dimensions ($d = 15\ \mu m$), the significance of Equation 4 relates to its ability to predict these factors from other experimental data.

Fig. 8a is a plot of the measured mirror constant versus fibre diameter. Despite appreciable scatter in the data, the mirror constant appears to increase with decreasing fibre diameter. A *t*-test was conducted on the data in Fig. 8a to better evaluate the apparent trend, and the data is shown to have a non-zero slope at a confidence level of 99%. The calculated slope is negative, suggesting that the mirror constant does, in fact, increase with decreasing fibre diameter. Fig. 8b shows the relationship between the mirror-to-fibre-size ratio (r_m/r) and the fibre diameter, demonstrating that this ratio does not vary with diameter. The critical flaw location is plotted as a function of fibre diameter in Fig. 8c. Although an obvious trend is not apparent in the plot, the data suggests that λ either increases slightly with decreasing diameter, or remains constant. Specifically, λ certainly does not decrease with decreasing diameter. If λ is constant with diameter, then the trends observed in Fig. 8 would suggest that the apparent fibre K_{1c} increases with decreasing fibre diameter. If λ increases slightly with decreasing diameter, the work by Kobayashi *et al.* [36] indicates that Y' increases with increasing λ, then Y' must increase with decreasing diameter, and consequently K_{1c} should increase with decreasing diameter with a stronger trend than that observed for A_m in Fig. 8a. Therefore, we can conclude from Fig. 8 that K_{1c} increases with decreasing diameter for Nicalon fibres.

Fig. 9 examines the effects of critical flaw location on fibre fracture. Due to the varying fibre diameters, flaw location is best characterized as a normalized parameter, λ. Fracture strength is plotted as a function of flaw location in Fig. 9a. Fibres that fracture due to flaws located near the centre of the fibre show lower average strengths than those failing due to outlying flaws, with mean strength increasing as normalized distance from fibre centre increases. It is also suggested that centrally-located flaws yield less scatter in strength than flaws existing closer to the surface. These apparent trends are in marked contrast to that observed between mirror constant and flaw location, as shown in Fig. 9b.

Here, the mirror constant is shown to remain constant with varying flaw location, suggesting that the ratio of K_{1c} to Y' is unaffected by changes in flaw position.

4. Discussion

Results presented in the previous section suggest that variations in both fibre diameter and flaw location may affect the fracture behaviour of Nicalon fibres. We have concluded from Fig. 8 that the apparent K_{1c} increases with decreasing diameter for Nicalon fibres. One possible explanation may be that smaller fibres possess intrinsically higher densities, greater purity and thus more homogeneous microstructures, and may therefore have higher K_{1c} values. Based upon findings by Yajima and co-workers [37], which showed a trend for increasing Young's modulus with decreasing fibre diameter, Andersson and Warren [1] suggested that fibres of higher purity SiC can be achieved at smaller diameters, possibly as a result of a more effective pyrolysis.

Although ceramic fibres typically yield significant variability in measurements of their mechanical properties, the scatter observed in each of Figs 8 and 9 is quite appreciable and requires further explanation. One potentially significant source of data variability stems from the structural inhomogeneities which exist in Nicalon fibres after processing. Following pyrolysis, Nicalon SiC fibres are shown to possess a predominantly amorphous Si–C–O matrix containing dispersed microcrystallites of β-SiC [1, 7, 17–21, 38, 39]. Oxygen resulting from the curing process is retained as SiO_2 across the fibre diameter, possibly accounting for 20–30% of the total fibre weight [1]. Excess carbon, in the form of graphite crystallites [40] or free-carbon segregates, is also found in the Nicalon fibres, representing approximately 10 wt% of the fibre [1]. Additionally, Lipowitz [39] has reported the presence of a pore phase of approximately 5–20 vol % in Nicalon fibres, and attributes this phase to the evolution of gaseous species during fibre pyrolysis. Butt [22] has reported that smaller diameter fibres may resist evolution of gaseous species because of inherently higher surface tensions, suggesting that the pore phase could potentially vary with fibre diameter.

None of the aforementioned microstructural phases has been observed to display any degree of regular periodicity throughout the fibre matrix. Thus, it is evident that Nicalon fibres possess inherently complex microstructures as a result of various stages in the processing. To our knowledge, no studies have been conducted to characterize fibre microstructure as a function of fibre diameter, nor as a function of location within the fibre, and thus the extent to which individual phases may vary with diameter and position is unknown. Given the limited data on this matter, we can only hypothesize that variations in microstructure do occur with both fibre diameter and location, and that these variations potentially contribute to the scatter observed in Figs 8 and 9.

The scatter observed in Fig. 8a may also be related to the presence of different flaw populations and to variations in critical flaw location, both of which can contribute to data scatter and thus affect mirror-constant values. Similarly, the moderate scatter observed in Fig. 8b is also attributable to several sources. The determination of Y' for fracture in a particular sample depends not only on the geometry and size of the specimen, but also on the size and location of the flaw. For bulk specimens of standard geometry and predetermined flaw shape, calculation of Y' is a fairly straightforward procedure as the flaw is assumed to be in a fixed location and to possess a known geometry. These assumptions, however, do not apply to the fracture of Nicalon fibres. As fractography of the fibres demonstrates, flaws do not occupy a fixed location, nor do they conform to a fixed geometry. Furthermore, deviations from circular cross-sections in Nicalon fibres result in a variety of different effective specimen geometries which further contribute to the scatter in Y' observed in Fig. 8.

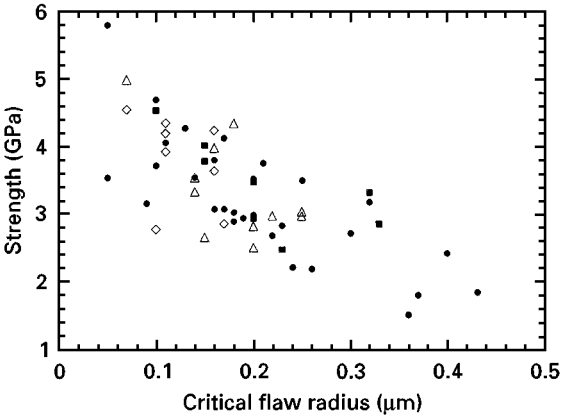

Figure 10 A plot of strength versus critical flaw size for all fibres reveals that fibre strength is more dependent on flaw size than on flaw type. (●) Surface flaw; (■) pore cluster; (△) granular defect; (◇) individual pore.

Contrary to results reported previously [20] for fracture of Nicalon fibres, none of the *interior* flaw populations examined in this study correlate to specific strength ranges, or show a specific strength–flaw size relationship. Rather, as Fig. 10 suggests, fibre strength appears to be more dependent on flaw size than on flaw type, as all of the flaw populations contribute to fracture over a broad spectrum of strength values. In Fig. 5, surface flaws were shown to be prevalent at small fibre diameters because of the high surface-to-volume ratio of the fibre. Fig. 11 reveals that surface flaws are also preferentially sampled over interior flaws at longer gauge lengths, where statistically weaker flaws dominate failure. Additionally, fractography reveals that the three interior flaw populations tend to occupy preferred locations in the fibres. This behaviour is illustrated in Figs 12, 13, and 14, where statistical calculations are used to obtain the accumulative flaw distribution (F), the associated flaw distribution (f), and the critical flaw density (p) as a function of critical flaw location (λ) for individual pores, pore clusters and granular defects, respectively.

The statistical distribution of flaw location for each of the three populations can be inferred from

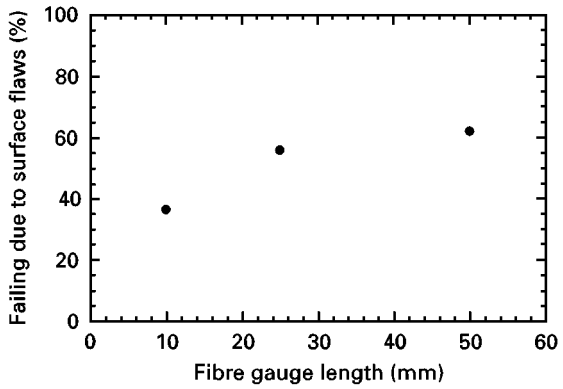

Figure 11 Percentage of fibres failing due to surface flaws as a function of fibre gauge length.

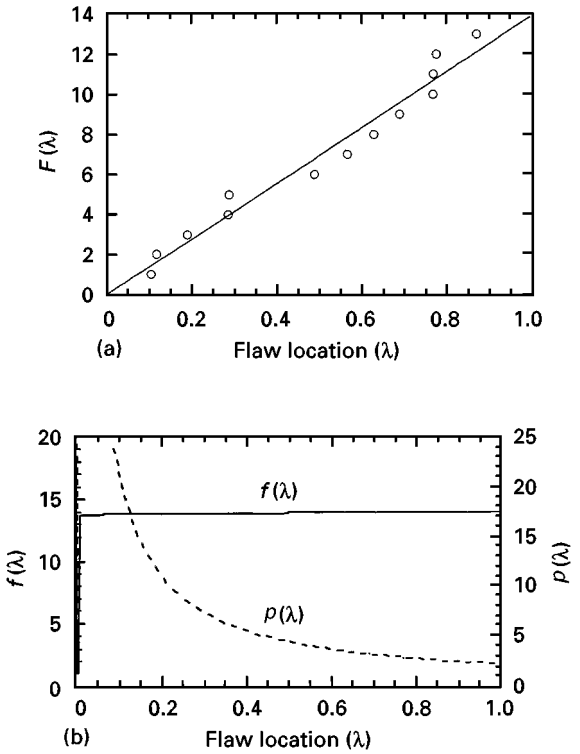

Figure 12 The (a) accumulative flaw distribution ($n = 1.0042$), as well as the (b) associated flaw distribution (solid line) and flaw density (dashed line), for individual pores with respect to flaw location.

Figs 12–14. For each flaw population, individual flaws are ranked in order of increasing λ. The accumulative flaw distribution function is obtained by plotting the normalized flaw locations in a given population, and then fitting the data to a power law of the form

$$F(\lambda) = A\lambda^n \tag{5}$$

where A and n are empirical constants. These curves are shown in part (a) of Figs 12–14. These figures demonstrate that very few critical flaws are located close to the fibre centre, as would be expected given the small volume that a flaw could potentially occupy if positioned at short distances from the fibre centre.

The associated flaw distribution is determined from the first derivative of $F(\lambda)$

$$f(\lambda) = nA\lambda^{n-1} \tag{6}$$

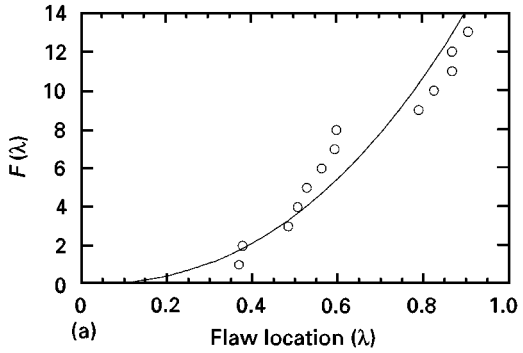

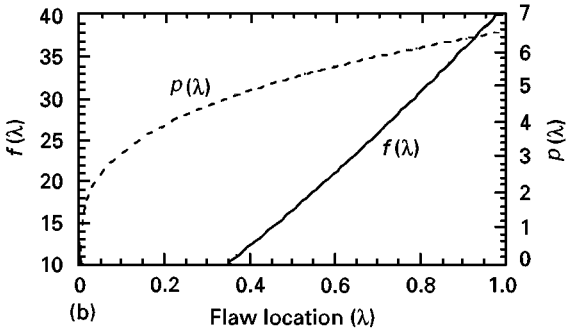

Figure 13 The (a) accumulative flaw distribution ($n = 2.3179$), as well as the (b) associated flaw distribution (solid line) and flaw density (dashed line), for pore clusters with respect to flaw location.

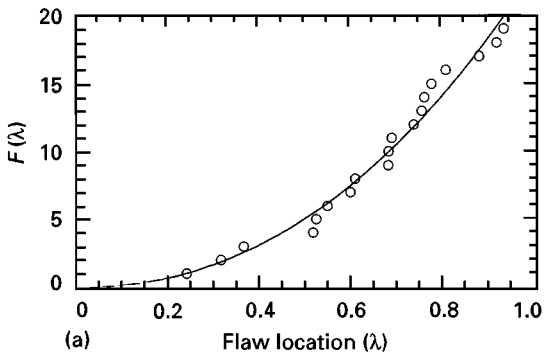

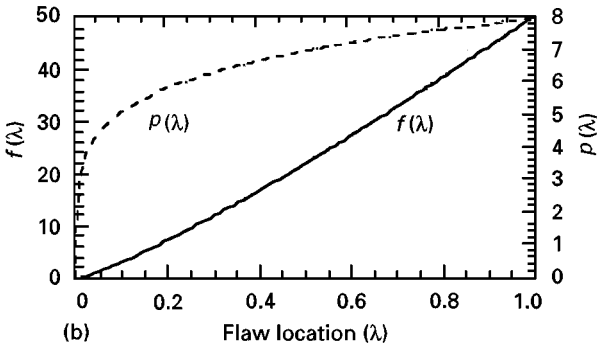

Figure 14 The (a) accumulative flaw distribution ($n = 2.195$), as well as the (b) associated flaw distribution (solid line) and flaw density (dashed line), for granular defects with respect to flaw location.

Physically, $f(\lambda)$ describes the distribution of flaws contained within an element (dλ) of the fibre volume, as illustrated in Fig. 15. Dividing $f(\lambda)$ by $2\pi\lambda$ yields the critical flaw density

$$p(\lambda) = \frac{nA\lambda^{n-2}}{2\pi} \tag{7}$$

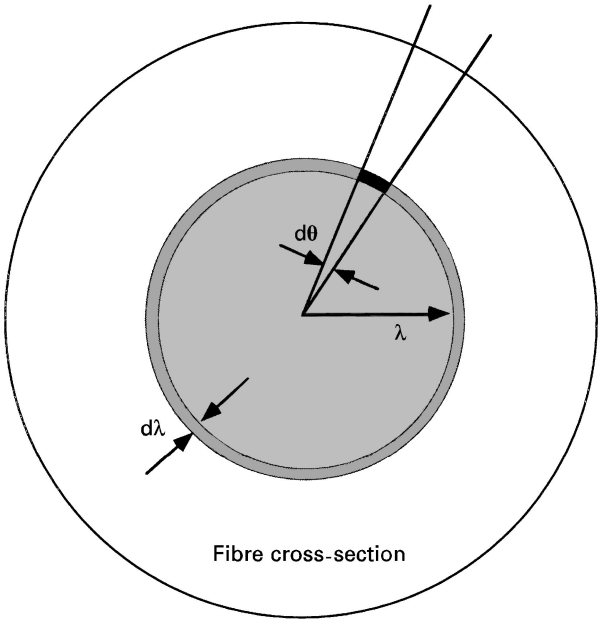

Figure 15 Schematic view of a fibre cross-section demonstrating the physical significance of each of the three statistical functions, $F(\lambda)$ (□), $f(\lambda)$ (▨), and $p(\lambda)$ (■) , used to characterize flaw population with respect to location.

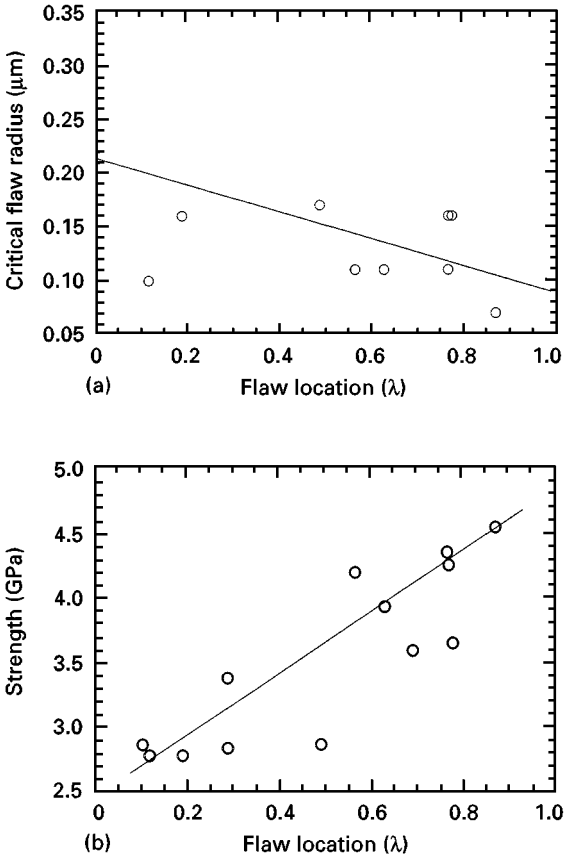

Figure 16 (a) Critical flaw size and (b) strength versus critical flaw location for fibres failing because of individual pores.

which represents the critical flaw distribution normalized to a specific volume of the fibre (see Fig. 15). This function, when integrated over the entire locus of normalized flaw location, yields $F(\lambda)$

$$\int_0^{\lambda} p(\lambda)\, 2\pi\lambda \mathrm{d}\lambda = F(\lambda) \tag{8}$$

Both $f(\lambda)$ and the critical flaw density $p(\lambda)$ are plotted as a function of critical flaw location in part (b) of Figs 12–14. These plots yield some intriguing results regarding the dependence of different flaw populations on critical flaw location.

Individual pores can be found throughout most of the fibre domain, and are primarily responsible for fracture occurring due to flaws located near the centre of the fibre. The solid line in Fig. 12b indicates that individual pores which serve as critical flaws remain equally distributed over the entire range of normalized fibre distance. The density of these critical flaws (dashed line) is highest at the fibre centre ($\lambda = 0$) and is seen to decrease with increasing λ. The only three data points existing below $\lambda = 0.2$ in Fig. 9a represent strength values for fibres fracturing due to individual pores. Little deviation in fracture strength ($\sigma = 2.78$, 2.78, and 2.87 GPa) is observed in these three fibres. Pore sizes generally tend to decrease as the normalized distance from fibre centre increases (Fig. 16a), causing associated strength values to increase (Fig. 16b). Fewer data points exist in Fig. 16a than in Fig. 16b because some of the pore sizes could not be accurately measured.

Critical flaws in the form of pore clusters and granular defects are found predominantly at larger values of λ. Both of these flaw populations have increasing $f(\lambda)$ with increasing distance from the fibre centre, as the solid lines in Figs 13b (pore clusters) and 14b (granular defects) illustrate. Moreover, critical flaw densities are shown to increase with increasing λ for both pore clusters and granular defects.

The demonstrated propensity for individual interior flaw populations to occupy select regions of the fibre may partially explain the trends observed in Fig. 9a. This figure shows the dependence of fracture strength on critical flaw location. Average strength values, as well as the overall scatter in strength, are seen to increase as the critical flaw location moves further away from the fibre centre ($\lambda = 0$). Although the variation in strength with flaw location could possibly be explained by changes in critical flaw size and fibre gauge length, another explanation is offered by the dependence of individual flaw populations on critical flaw location. Close to the fibre centre, only one type of critical flaw is likely to exist – the individual pore – and at low λ values, this population is shown to have very little variation in strength values. However, moving further away from the fibre centre, all three interior flaw populations could potentially serve as fracture initiators, which could possibly explain why the scatter in strength becomes so large with increasing λ.

5. Conclusions

The strength and fracture behaviour of Nicalon fibres ranging in diameter from 8 to 22 μm have been characterized using extensive fractographic analysis. Results suggest that variations in both fibre diameter and flaw location can influence the mechanical response of

fibres fractured under tensile loading. As fibre diameter decreases, the apparent fibre fracture toughness (K_{1c}) appears to moderately increase. Tensile strength is shown to vary with flaw location, with higher strengths accompanying flaws located further away from the fibre centre. Larger scatter in strength values is also observed with increasing distance from fibre centre. This scatter has been attributed primarily to variations in critical flaw population with varying flaw location. Individual pores are seen to be distributed throughout the fibre domain, and are primarily responsible for fracture occurring due to flaws located closest to the fibre centre. Pore clusters and granular defects are located predominantly in the outer regions of the fibre. The individual flaw populations are not observed to correlate to specific fibre strength values, suggesting that flaw size, and not flaw type, plays a more prominent role in determining fibre strength values.

This work is expected to have relevant implications to other types of ceramic fibres derived from polymeric precursors which are likely to possess inherently broad distributions of fibre diameters.

Acknowledgements

This work was supported by the Laboratory Directed Research and Development Office and by the Director's Postdoctoral Fellowship Program of Los Alamos National Laboratory. This work was performed at Los Alamos National Laboratory under the auspices of the US Department of Energy (contract W-7405-EN-36).

References

1. H. ANDERSSON and R. WARREN, *Composites* **15** (1984) 16.
2. T. MAH, N. L. HECHT, D. E. McCULLUM, J. R. HOENIGMAN, H. M. KIM, A. P. KATZ and H. A. LIPSITT, *J. Mater. Sci.* **19** (1984) 1191.
3. T. J. CLARK, R. M. ARONS, J. B. STAMATOFF and J. RABE, *Ceram. Engng Sci. Proc.* **7** (1985) 576.
4. A. S. FAREED, P. FANG, M. J. KOCZAK and F. M. KO, *Amer. Ceram. Soc. Bull.* **66** (1987) 353.
5. H. E. KIM and A. J. MOORHEAD, *J. Amer. Ceram. Soc.* **74** (1991) 666.
6. G. EMIG and R. WIRTH, *J. Mater. Sci.* **30** (1995) 5813.
7. A. R. BUNSELL and G. SIMON, *Comp. Sci. Technol.* **27** (1986) 157.
8. T. MAH, M. G. MENDIRATTA, A. P. KATZ, R. RUH and K. S. MAZDIYASNI, *J. Amer. Ceram. Soc.* **68** (1985) C27.
9. K. M. PREWO, *J. Mater. Sci.* **21** (1986) 3590.
10. M. D. THOULESS, O. SBAIZERO, L. S. SIGL and A. G. EVANS, *J. Amer. Ceram. Soc.* **72** (1989) 525.
11. A. J. ECKEL and R. C. BRADT, *ibid.* **72** (1989) 455.
12. D. S. BEYERLE, S. M. SPEARING, F. W. ZOK and A. G. EVANS, *ibid.* **75** (1992) 2719.
13. D. SINGH and J. P. SINGH, *Ceram. Engng Sci. Proc.* **13** (1992) 257.
14. B. J. NORMAN, A. C. JARAS and J. ASHALL, *Brit. Ceram. Trans.* **92** (1993) 62.
15. W. A. CURTIN, *J. Amer. Ceram. Soc.* **77** (1994) 1075.
16. C. H. ANDERSSON and R. WARREN, in "Advances in composite materials," edited by A. R. Bunsell, C. Bathias, A. Martrenchar, D. Menkes, and G. Verchery (Pergamon Press, Oxford, 1980) p. 1129.
17. G. SIMON and A. R. BUNSELL, *J. Mater. Sci.* **19** (1984) 3649.
18. *Idem.*, *Sci. Ceram.* **12** (1984) 647.
19. L. C. SAWYER, R. ARONS, F. HAIMBACH, M. JAFFE and K. D. RAPPAPORT, *Ceram. Engng Sci. Proc.* **6** (1985) 567.
20. L. C. SAWYER, M. JAMIESON, D. BRIKOWSKI, M. ISHAQ HAIDER and R. T. CHEN, *J. Amer. Ceram. Soc.* **70** (1987) 798.
21. S. YAJIMA, K. OKAMURA, J. HAYASHI and M. OMORI, *ibid.* **59** (1976) 324.
22. D. P. BUTT, Bachelor thesis, Department of Materials Science and Engineering, Pennsylvania State University, University Park, PA, 1984.
23. G. D. SORARU, M. MERCADINI and R. DAL MASCHIO, *J. Amer. Ceram. Soc.* **76** (1993) 2595.
24. S. L. PHOENIX and R. G. SEXSMITH, *J. Comp. Mater.* **6** (1972) 322.
25. E. G. STONER, D. D. EDIE and S. D. DURHAM, *J. Mater. Sci.* **29** (1994) 6561.
26. E. B. SHAND, *J. Amer. Ceram. Soc.* **42** (1959) 474.
27. M. J. KERPER and T. G. SCUDERI, *Amer. Ceram. Soc. Bull.* **43** (1964) 622.
28. W. C. LEVENGOOD, *J. Appl. Phys.* **29** (1958) 820.
29. J. J. MECHOLSKY, S. W. FREIMAN and R. W. RICE, *J. Mater. Sci.* **11** (1976) 1310.
30. *Idem.*, in "Fractography in failure analysis, ASTM STP 645," edited by B. M. Strauss and W. H. Cullen, Jr (American Society for Testing and Materials, West Conshohocken, PA, 1978) p. 363.
31. H. P. KIRCHNER and R. M. GRUVER, in "Fracture mechanics of ceramics," Vol. 1, edited by R. C. Bradt, D. P. H. Hasselman, and F. F. Lange (Plenum Press, New York, 1974) p. 309.
32. J. J. MECHOLSKY, R. W. RICE and S. W. FREIMAN, *J. Amer. Ceram. Soc.* **57** (1974) 440.
33. D. A. KROHN and D. P. H. HASSELMAN, *ibid.* **54** (1971) 411.
34. K. R. McKINNEY, *ibid.* **56** (1973) 225.
35. D. BROEK, "Elementary Engineering Fracture Mechanics" 4th Revised Edn (Martinus Nijhoff Publishers, Dordrecht, The Netherlands, 1986) p. 18.
36. A. S. KOBAYASHI, M. ZIV and L. R. HALL, *Int. J. Fract. Mech.* **1** (1965) 81.
37. S. YAJIMA, M. OMORI, J. HAYASHI, K. OKAMURA, T. MATSUZAWA and C. LIAW, *Chem. Lett., Chem. Soc. Japan* **1976** (1976) 551.
38. R. CHAIM, A. H. HEUER and R. T. CHEN, *J. Amer. Ceram. Soc.* **71** (1988) 960.
39. J. LIPOWITZ, *Amer. Ceram. Soc. Bull.* **70** (1991) 1888.
40. S. YAJIMA, K. OKAMURA, T. MATSUZAWA, Y. HASEGAWA and T. SHISHIDO, *Nature* **279** (1979) 706.

Received 29 April
and accepted 24 September 1997